

# Pure gauge QCD Flux Tubes and their widths at Finite Temperature

P. Bicudo,<sup>\*</sup> N. Cardoso,<sup>†</sup> and M. Cardoso<sup>‡</sup>

*CFTP, Departamento de Física, Instituto Superior Técnico (Universidade  
Técnica de Lisboa), Av. Rovisco Pais, 1049-001 Lisboa, Portugal*

We study the flux tubes produced by static quark-antiquark, quark-quark and quark-gluon charges at finite temperature in pure gauge SU(3) lattice QCD. Our sources are static and our lattice correlators are composed of fundamental and adjoint Polyakov loops. To signal the flux tubes, we compute the square densities of the chromomagnetic and chromoelectric fields with plaquettes, in a gauge invariant framework. We study the existence and non-existence of flux tubes both above and below the deconfinement phase transition temperature  $T_c$ . Using the Lagrangian density as a probability distribution, we also compute the widths of the flux tubes and study their widening as a function of the interchange distance. We determine our results with both statistical and systematic errors. Our computations are performed in NVIDIA GPUs using the CUDA language.

## I. INTRODUCTION

The understanding of confinement and deconfinement in QCD remains a central problem of particle physics. A major evidence of QCD confinement is the flux tube arising between quark-antiquark static charges, both from gauge invariant pure gauge lattice QCD simulations [1–4] and from experimental observations like Regge trajectories [5–9] consistent with linear confining potentials. Even in dynamical QCD where the flux tube breaks due to the creation of another quark and antiquark, a flux tube develops up to moderate quark-antiquark distances. Different flux tubes have also been shown to occur in lattice QCD simulations of different exotic hadrons, typical of SU(3) [10–13]. It is important for the fundamental understanding of the pure gauge QCD flux tubes to measure the flux tube profile [14–20] with more quantitative results.

In this work, we study whether flux tubes exist or not, between different static charges, at different temperatures above and below pure gauge QCD critical deconfinement temperature  $T_c$ . In particular, we study the flux tubes created between static quark-antiquark, quark-quark and quark-gluon charges.

Notice we do not know exactly, neither the theoretical origin of the QCD flux tubes nor their effective behavior, and it is important to explore in more detail their properties in order to, hopefully, one day solve this important problem. For instance, two qualitatively different effective models for the QCD flux tube exist.

Already in the 1970's, Nambu [21], 't Hooft [22] and Mandelstam [23] proposed that quark confinement would be physically interpreted using the dual version of the superconductivity [24, 25]. The QCD vacuum state would behave like an ordinary superconductor, where Cooper-pair condensation leads to the Meissner effect, and the magnetic flux is excluded from the vacuum and squeezed

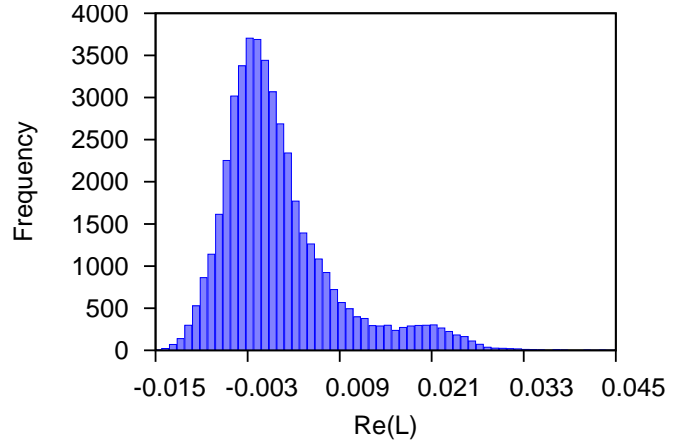


Figure 1: (Colour Online.) Histogram of the Polyakov loop history for  $\beta = 6.055$  [43].

in a quasi-one-dimensional tube, the Abrikosov-Nielsen-Olesen vortex, where the magnetic flux is quantized topologically [26–28]. In a superconductor, the fields are approximately classical and the flux tube main parameter is the penetration length  $\lambda$  in the London equation has a direct relation with an effective mass of the interaction particle fields, i. e., the photon. In QCD, the dual gluon mass has been studied by several authors, [29–36], as well as the gluon effective mass [37]. Interestingly, there is also an evidence for a gluon mass in the Landau Gauge [38] and in the multiplicity of particles produced in heavy ion collisions [39]. Recently, the penetration length started to be computed with gauge invariant lattice QCD techniques [40–42].

On the other extreme limit, at quark-antiquark distances larger than the penetration length, the flux tube is similar to a quantum string, contrary to the picture of the superconductor with classical electromagnetic fields. Due to its vibration, the quantum string has a Gaussian profile and a finite width, different from the exponential profile of the classical superconductor flux tube [45, 46]. Thus a second model of the QCD flux tube is given by the string model, based on the Nambu-Goto Action [47, 48].

At zero temperature, the energy of the quantum string

<sup>\*</sup> bicudo@tecnico.ulisboa.pt

<sup>†</sup> nuno.cardoso@tecnico.ulisboa.pt

<sup>‡</sup> mjdc@cfpt.ist.utl.pt

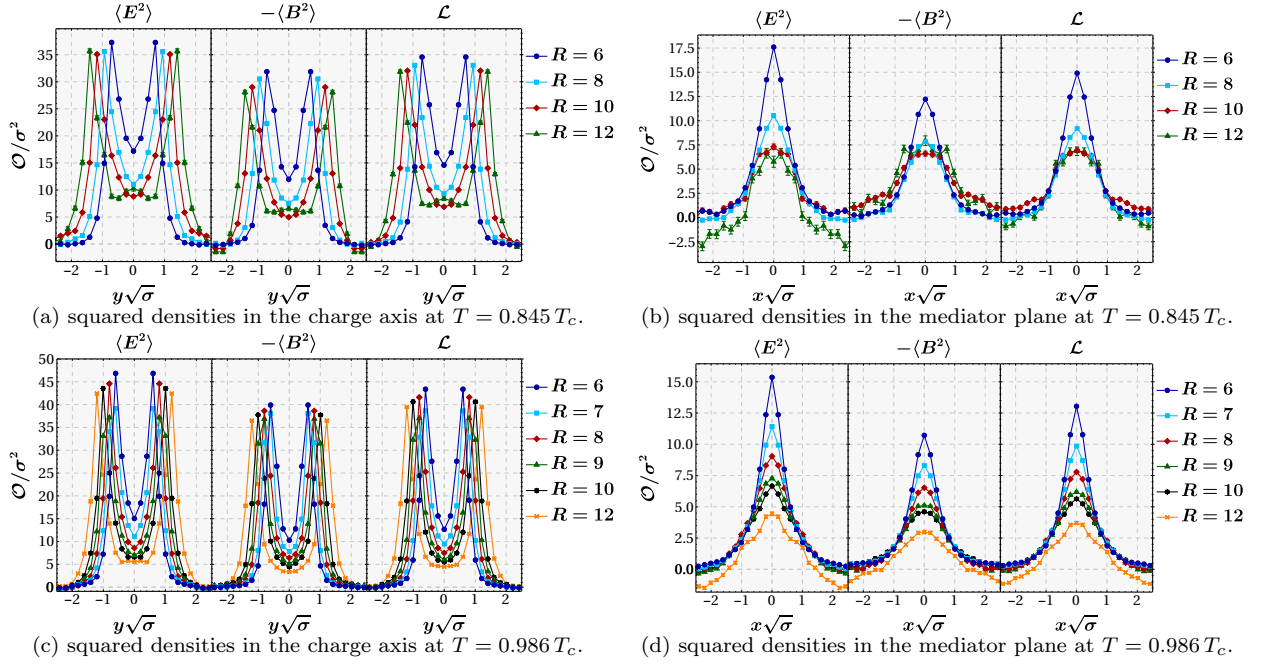


Figure 2: (Colour Online.) Results for the chromoelectric field, chromomagnetic field and action density for the  $Q\bar{Q}$  system at  $T \leq T_c$ .

Volume	$\beta$	$T/T_c$	$a\sqrt{\sigma}^{[44]}$	# config.
$32^4$	6.0	0	0.219718	1100
$48^3 \times 8$	5.96	0.845	0.235023	5990
$48^3 \times 8$	6.0534	0.986	0.201444	5990/5110*
$48^3 \times 8$	6.13931	1.127	0.176266	5990
$48^3 \times 8$	6.29225	1.408	0.141013	5990
$48^3 \times 8$	6.4249	1.690	0.117513	5990

Table I: Lattice ensembles, in  $48^3 \times 8$  volumes at finite  $T$  and in a  $32^4$  volume at  $T = 0$ . We denote with an \* the number of remaining configurations after we remove the configurations contaminated by the other phase.

with length  $R$  and fixed ends, with quantum transverse fluctuations quantum number  $n$ , is expressed in the Lüscher term and in the Arvis Potential [49, 50],

$$\begin{aligned}
 V_n(R) &= \sigma \sqrt{R^2 + \frac{2\pi}{\sigma} \left(n - \frac{D-2}{24}\right)} \\
 &= \sigma R + \frac{\pi}{R} \left(n - \frac{D-2}{24}\right) + \dots
 \end{aligned} \quad (1)$$

indeed observed in lattice QCD for 4 space-time dimensions [45]. In Eq. (1),  $D$  is the dimension of the space time. Note that the Arvis potential is tachyonic at small distances since the argument of the square root becomes negative in this limit, moreover rotational invariance is only achieved for  $D = 26$ . Nevertheless, the first two terms in the  $1/R$  expansion,  $\sigma R + \pi(n - \frac{D-2}{24})\frac{1}{R}$ , are

more general than the Arvis potential, since they fit the  $D = 3$  and  $D = 4$  lattice data quite well down to distances much smaller than the Arvis tachyonic distance. The  $1/R$  term is independent of the string tension  $\sigma$  and for the physical  $D = 3 + 1$  has the value  $-\frac{\pi}{12}$ . This is the Lüscher term [49]. The energy spectrum of a static quark-antiquark and of its flux tube is certainly well defined (not tachyonic) and this was the first evidence of flux tube vibrations found in lattice field theory. Moreover it was shown [45] that the width of the ground state flux tube diverges when  $R \rightarrow \infty$  with a logarithmic law,

$$w^2 \sim w_0^2 \log \frac{R}{R_0} \quad (2)$$

where the squared width  $w^2$  is the mean squared radius of the flux tube, computed in its centre. This enhancement of the flux tube transverse radius as  $R \rightarrow \infty$  is frequently denominated *widening*. The widening has been recently extended with two-loop calculations [51]. The flux tube widening has been verified numerically for compact U(1) QED  $D = 2 + 1$  lattices [52], for non-abelian SU(2)  $D = 2 + 1$  lattices [53–69] and, more recently, for the more physical four-dimensional SU(3) case [70, 71]. Recently, it has been shown the flux tubes exhibit characteristics of both superconductor and string models, with both a penetration length  $\lambda$  and the quantum widening of  $w$  [42].

Moreover, at finite  $T$ , close to  $T_c$  but still in the confining regime of  $T < T_c$ , it has been predicted in Ref. [72] that widening becomes linear with the intercharge distance  $R$ . This occurs because the flux tube width  $w$  also depends on the extent  $\tau$  of the compactified time

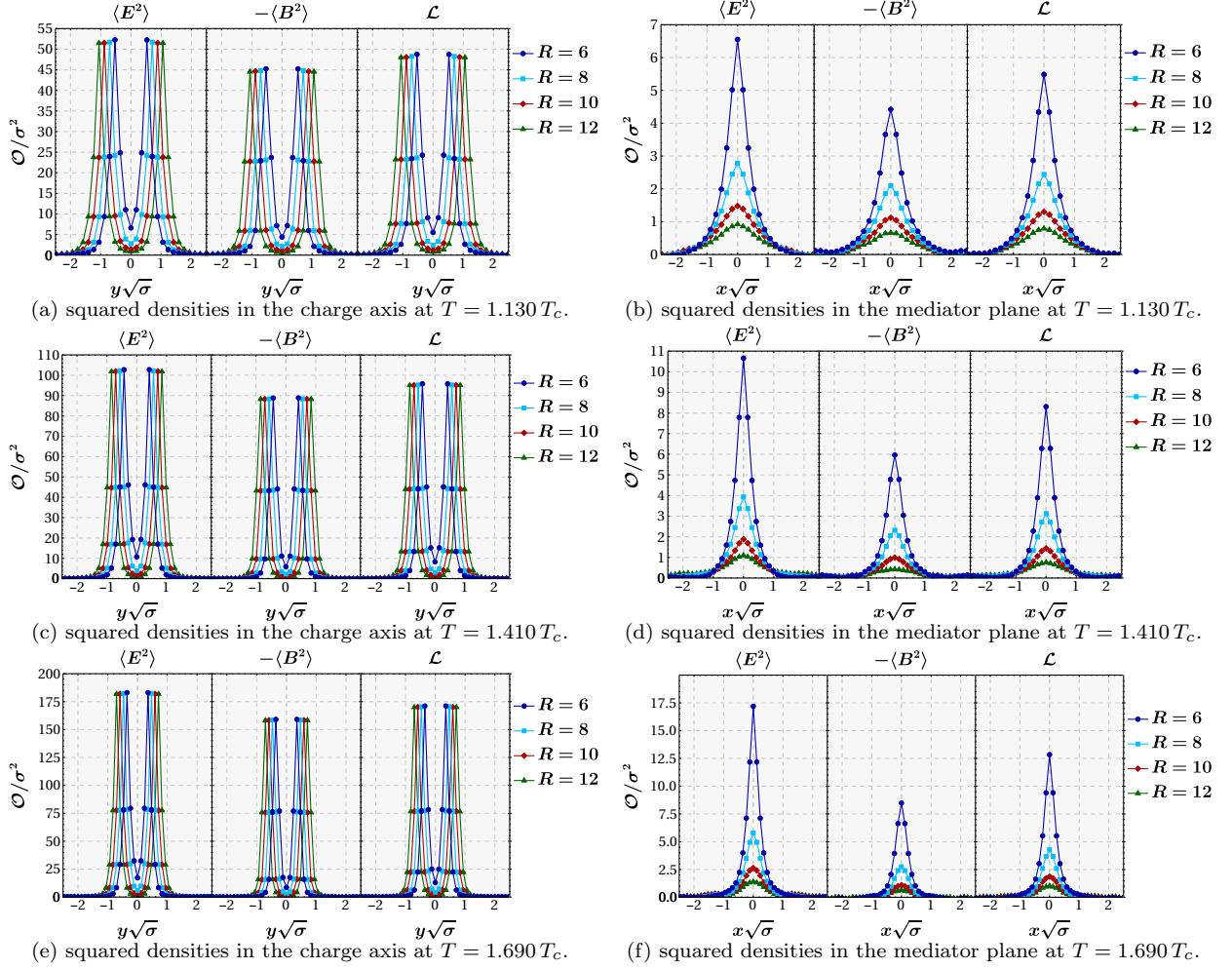


Figure 3: (Colour Online.) Results for the chromoelectric field, chromomagnetic field and action density for the  $Q\bar{Q}$  system at  $T > T_c$ .

distance of the lattice,

$$\sigma w^2 = \frac{1}{2\pi} \log \frac{\tau}{\tau_c} + \frac{R}{4\tau} - \frac{1}{\pi} e^{-2\pi \frac{R}{\tau}} + \dots \quad (3)$$

Since  $\tau$  is small at finite  $T$ , we expect the dominant term to be the linear term in  $R$ . This result has been verified for the Ising model [72] and for compact  $U(1)$  [52]. Recently, widening for  $SU(3)$  has also been studied for Baryons [70, 73, 74]. We intend to test the linear broadening of Eq. (3) as well for  $SU(3)$ .

However, at  $T > T_c$ , it has been recently claimed by Refs. [75, 76] that a flux tube continues to exist. This apparently contradicts previous results on the static quark-antiquark  $Q\bar{Q}$  potentials which indicate that linear confinement disappears for  $T > T_c$  [77]. Thus, we also intend to clarify how the color fields and possible flux tubes behave above the phase transition.

Here we extend our previous study [42] to finite temperature  $T$ . We aim to measure in detail with lattice QCD techniques the profile of  $SU(3)$  pure gauge flux tubes in dimensions  $D = 3 + 1$ . We study the color fields

distributions inside the flux tubes formed by Polyakov loops in the static  $Q\bar{Q}$ ,  $QQ$  and  $QG$  systems at finite  $T$ , both below and above the phase transition temperature  $T_c$ . We address how the flux tube evolves with the distance between quarks and when the temperature increases beyond the phase transition. Moreover, we compare our results with the  $T = 0$  flux tubes with the static  $Q\bar{Q}$  system computed with the Wilson loop [42]. In Section II, we describe the lattice formulation at finite  $T$ . We briefly review the Polyakov loops of the different color charges systems, detail how to compute the color field and Lagrangian distributions, and discuss the techniques we utilize to increase the signal over noise ratio. In Section III, we show our results for the different flux tube profiles and qualitatively discuss them. In Section IV, we compute and analyze the widening of the  $Q\bar{Q}$  flux tube profile in the intercharge mediator plane when the separation of the charges increase, in particular we analyze the systematic errors of the width and combine them with the statistical errors. Finally, we present our conclusion in Section V.

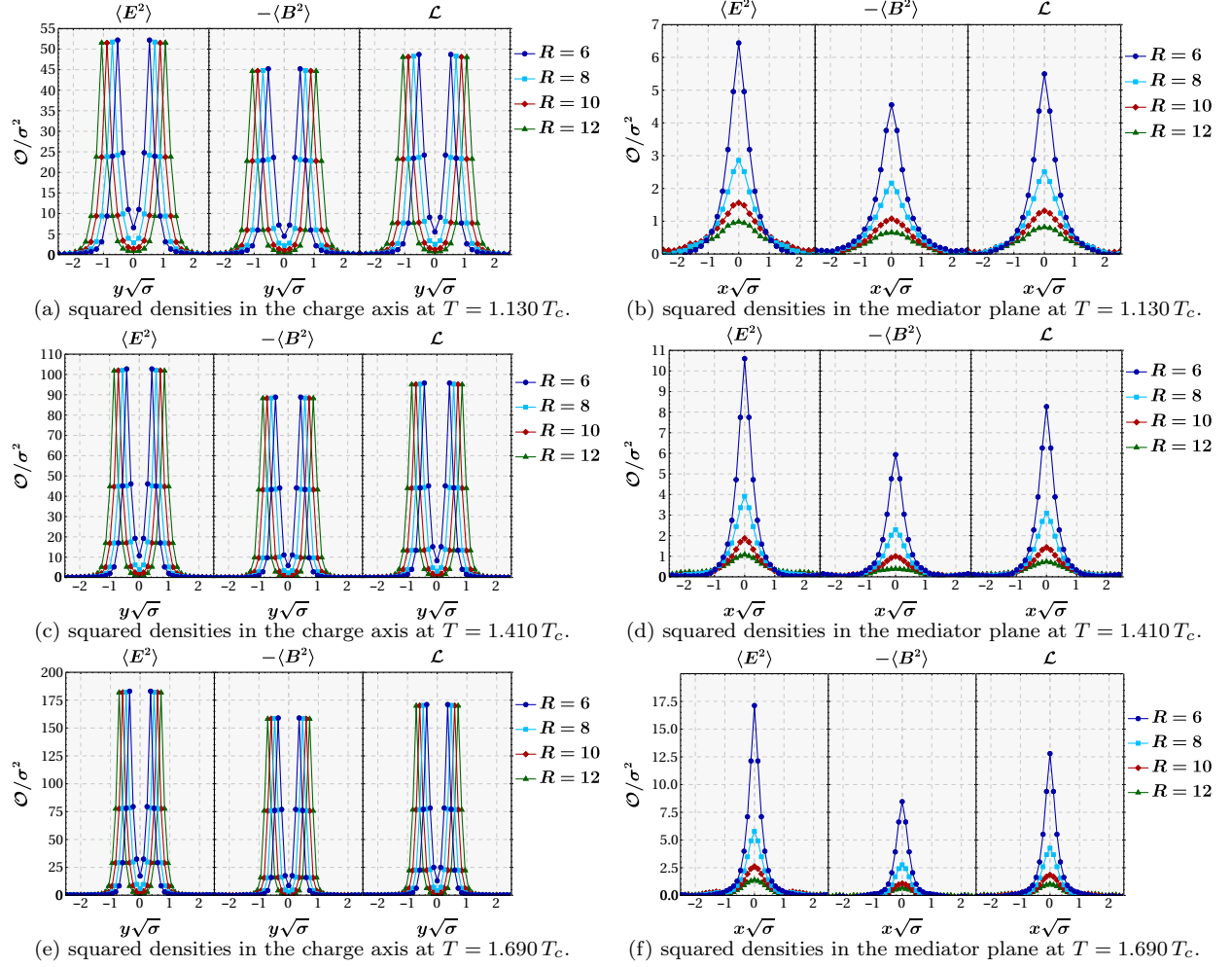


Figure 4: (Colour Online.) Results for the chromoelectric field, chromomagnetic field and action density for the  $QQ$  system.

## II. SU(3) LATTICE QCD FRAMEWORK

The relevant observables of the flux-tube system can be extracted from the correlation of the plaquette,  $\square_{\mu\nu}$ ,

$$\square_{\mu\nu}(x) = \frac{1}{3} \text{Tr} [U_\mu(x) U_\nu(x + \mu) U_\mu^\dagger(x + \nu) U_\nu^\dagger(x)] , \quad (4)$$

with the Polyakov loops,  $L$ . To reduce the fluctuations of the correlator  $\mathcal{O} \square_{\mu\nu}(x)$ , we measure the following quantity, [78],

$$f_{\mu\nu}(\mathbf{R}, \mathbf{r}) = \frac{\beta}{a^4} \left[ \frac{\langle \mathcal{O} \square_{\mu\nu}(\mathbf{r}) \rangle - \langle \mathcal{O} \square_{\mu\nu}(\mathbf{r}_{\text{ref}}) \rangle}{\langle \mathcal{O} \rangle} \right] , \quad (5)$$

where  $\mathbf{r}$  denotes the distance of the plaquette from the line connecting sources and  $\mathbf{r}_{\text{ref}}$  is an arbitrary reference point placed far from the sources. Our operators  $\mathcal{O}$  are combinations of fundamental representation Polyakov

loops  $L$ ,

$$\begin{aligned} \mathcal{O} &= L(-\mathbf{R}/2) L^\dagger(\mathbf{R}/2) && \text{for the } Q\bar{Q} \text{ system} , \\ \mathcal{O} &= L(-\mathbf{R}/2) L(\mathbf{R}/2) && \text{for the } QQ \text{ system} , \\ \mathcal{O} &= \left[ L(-\mathbf{R}/2) L^\dagger(-\mathbf{R}/2) - 1 \right] L(\mathbf{R}/2) && \text{for the } QG \text{ system} . \end{aligned} \quad (6)$$

Moreover,  $R$  is the separation between the sources,

$$L(\mathbf{R}/2) = \frac{1}{3} \text{Tr} \Pi_{t=1}^{N_t} U_4(\mathbf{R}/2, t) \quad (7)$$

is the fundamental Polyakov loop and  $N_t$  is the number of time slices of the lattice. We also use the periodicity in the time direction for the Polyakov loops to average the plaquette over the time direction,

$$\square_{\mu\nu}(\mathbf{r}) = \frac{1}{N_t} \sum_{t=1}^{N_t} \square_{\mu\nu}(\mathbf{r}, t) . \quad (8)$$



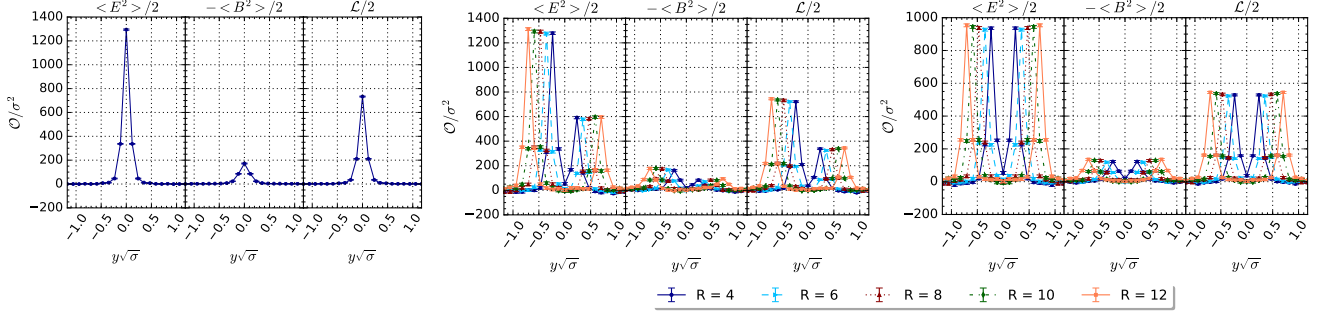


Figure 5: (Colour Online.) Charge axis squared field densities for the (left) single gluon  $G$  system, (center) gluon-quark  $QG$  system and (right) gluon-gluon  $GG$  system, both for  $\beta = 6.4249$ ,  $T = 1.690T_c$ .

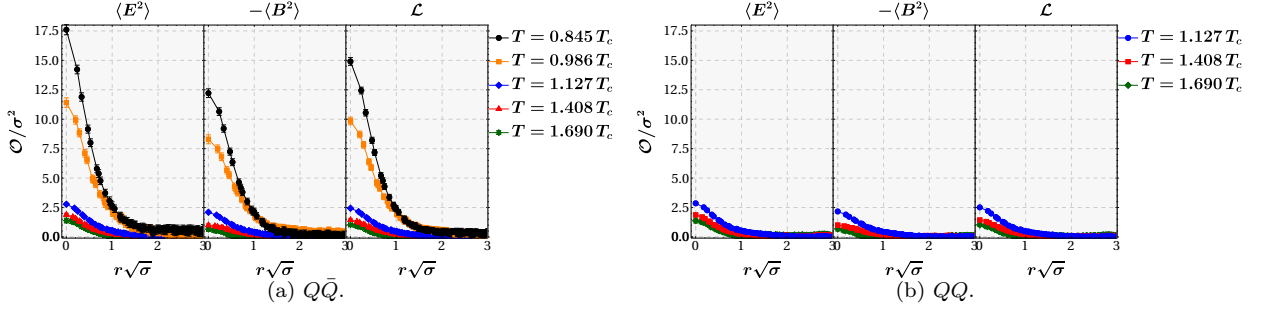


Figure 6: (Colour Online.) Flux profile in the mediator plane for  $R = 1.41\sqrt{\sigma}$ , left for the  $Q\bar{Q}$  pair and right for a  $QQ$  pair. Above the phase transition, the  $QQ$  and  $Q\bar{Q}$  squared field densities are almost identical modulo error bars.

Therefore, using the plaquette orientation  $(\mu, \nu) = (2, 3), (1, 3), (1, 2), (1, 4), (2, 4), (3, 4)$ , we can relate the six components in Eq. (5) to the components of the chromoelectric and chromomagnetic fields,

$$f_{\mu\nu} \rightarrow \frac{1}{2} (-\langle B_x^2 \rangle, -\langle B_y^2 \rangle, -\langle B_z^2 \rangle, \langle E_x^2 \rangle, \langle E_y^2 \rangle, \langle E_z^2 \rangle), \quad (9)$$

and also calculate the total action (Lagrangian) density,

$$\langle \mathcal{L} \rangle = \frac{1}{2} (\langle E^2 \rangle - \langle B^2 \rangle). \quad (10)$$

In order to improve the signal over noise ratio in the  $Q\bar{Q}$  and  $QQ$  systems, we use the extended multihit technique detailed in Ref. [42], which is an extended version of the multihit technique from [79, 80]. The technique consists in replacing each temporal link by its thermal average with the first  $N$ th order neighbors fixed. rather than just taking the thermal average of a temporal link with the first neighbors. We apply the heat-bath algorithm to all the links inside, averaging the central link,

$$U_4 \rightarrow \bar{U}_4 = \frac{\int [\mathcal{D}U_4]_{\Omega} U_4 e^{\beta \sum_{\mu,s} \text{Tr}[U_{\mu}(s)F^{\dagger}(s)]}}{\int [\mathcal{D}U_4]_{\Omega} e^{\beta \sum_{\mu,s} \text{Tr}[U_{\mu}(s)F^{\dagger}(s)]}}. \quad (11)$$

By using  $N = 2$  we are able to greatly improve the signal, when compared with the error reduction achieved with the simple multihit. Of course, this technique is more

computer intensive than simple multihit, while being simpler to implement than multilevel. The only restriction is  $R > 2N$  for this technique to be valid.

Moreover, just below the phase transition, we need to make sure that we don't have contaminated configurations as already mentioned in [43]. By plotting the histogram of Polyakov loop history for  $\beta = 6.055$ , Fig. 1, we are able to identify a second peak, and thus we remove all the configurations that lie on the second peak [43]. Therefore, in Table I the value with asterisk corresponds to the configurations after removing these contaminated configurations.

### III. RESULTS FOR THE SQUARED FIELD DENSITIES IN THE AXIAL AND MEDIATOR PLANES

In this section, we present the results for different  $\beta$  values using a fixed lattice volume of  $48^3 \times 8$ , our ensembles are detailed in Table I. We compute the lattice spacing, in units of the string tension at zero temperature, using the parametrization of Ref. [44]. All our computations are fully performed in NVIDIA GPUs using our CUDA language.

The two charges,  $Q\bar{Q}$  or  $G$ , are located at  $(0, -R/2, 0)$  and  $(0, R/2, 0)$  for  $R$  between 4 and 14 in lattice spacing units at  $T=0$ , and at finite  $T$  we start at  $R = 6$  and stop at  $R = 12$ . For  $\beta = 6.0534$ , we also study odd values,

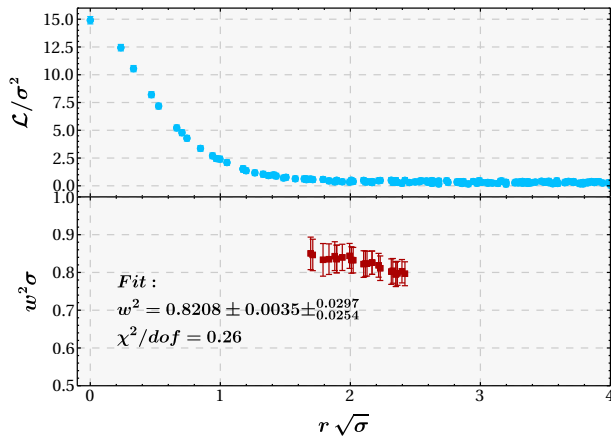


Figure 7: (Colour Online.) The profile of the flux tube Lagrangian density  $\mathcal{L}$  as a function of  $r$  (top) and the flux tube width  $w$  as a function of  $r_{\max}$  (bottom), with statistical errors, are illustrated for  $\beta = 5.96$  and  $R = 6a$ . We consider the interval  $r_{\max} \in [r(\mathcal{L}_0/50), r(\mathcal{L}_0/500)]$ . The statistical error bars of the width  $w$  are computed with the average, maximum and minimum values of  $w$  in the interval.

$R = 7$  and  $9$ .

Our results consist in the squared field densities in two planes, the axial plane including the two charges, and the mediator plane of the two charges.

In Figs. 2 and 3, we show the results for the  $Q\bar{Q}$  system. As expected the strength of the fields decrease with the temperature. In Fig. 4, we show the results for the  $QQ$  system at  $T > T_c$  (below  $T_c$  the Polyakov loop of non color-singlet systems vanish). It is remarkable that these results are almost identical, modulo statistic errors, to the ones of the  $Q\bar{Q}$  system. We interpret this as an evidence the imaginary part of the Polyakov loops is vanishing, since the Polyakov loop and anti-loop are Hermitian conjugate, as in Eq. 6, and thus only differ in the imaginary part.

Moreover, in Fig. 5 we study the effect of including a static gluon in the system with an adjoint Polyakov loop detailed in Eq. 6.

As in the case with quark sources  $QQ$  and  $Q\bar{Q}$  only, we find evidence the total square fields of the  $QG$  system are approximately similar to a simple linear sum of the square fields produced by two charges. We find this linear superposition contradicts the existence of flux tubes at  $T > T_c$ , since flux tubes are clearly non-linear objects.

#### IV. ANALYSIS OF TUBE WIDENING, INCLUDING SYSTEMATIC ERRORS

In this section, we analyze the flux tube profiles in the mediator plane, equidistant between the charges. Examples of profiles are shown in Fig. 6, where we compare the  $Q\bar{Q}$  and  $QQ$  profiles. We make use of the axial dis-

$R$	$R\sqrt{\sigma}$	$w^2(R/2)\sigma$	combined error
6	1.4101	0.820834(35) $\left(\frac{297}{254}\right)$	0.0310
8	1.8802	0.889802(18) $\left(\frac{451}{239}\right)$	0.0363
10	2.3502	0.956235(27) $\left(\frac{1085}{440}\right)$	0.0790
12	2.8203	1.16461(19) $\left(\frac{1455}{669}\right)$	0.1081

Table II: Results for the flux tube width with statistical and systematic errors, in the case of  $\beta = 5.96$ .

crete symmetry to increase the statistics of points with equal distance  $r = \sqrt{x^2 + z^2}$  to the axial charge axis  $y$ .

At  $T$  below  $T_c$  only the color singlet  $Q\bar{Q}$  system produces finite Polyakov loops. Moreover, at  $T$  above  $T_c$  the profiles are simply additive, in the sense the  $QQ$  profile is almost identical to the  $Q\bar{Q}$  profile, as discussed in Section III. Thus, in this Section, we specialize in the profiles of the  $Q\bar{Q}$  system only. Moreover, we combine the squared field densities in the Lagrangian density to get a clearer signal, with smaller statistical errors. Our main concern is to compute quantitative results from the profiles for different temperatures  $T$  and intercharge distances  $R$ .

We first fit the flux tube profile with the ansatz proposed in Ref. [42],

$$F^2(r) = F_0^2 \exp\left(-\frac{2}{\lambda}\sqrt{r^2 + \nu^2} + 2\frac{\nu}{\lambda}\right) + \mathcal{K}, \quad (12)$$

with three physical parameters: the axis central intensity of the flux tube  $F_0^2$ , the penetration length at large distances from the axis  $\lambda$  and the parameter  $\nu$  related to the second derivative  $-2F_0^2/(\lambda\nu)$ . We also have the unphysical parameter  $\mathcal{K}$  which is due to the statistical fluctuations of the fields at the reference point  $x_R$  of Eq. (5). This is a small parameter, vanishing for high statistics.

Moreover, with our fit we also compute another quantitative parameter [42], considering the normalized  $[F^2(r) - \mathcal{K}]$  as a probability density, the root mean square width,  $w = \sqrt{\langle r^2 \rangle}$ , of the flux tube profile,

$$\begin{aligned} w^2 &= \frac{\int_0^\infty r^3 [F^2(r) - \mathcal{K}] dr}{\int_0^\infty r [F^2(r) - \mathcal{K}] dr} \\ &= \frac{3}{2}\lambda^2 + 2\frac{\lambda\nu^2}{\lambda + 2\nu}. \end{aligned} \quad (13)$$

To compute the width,  $w$ , which is the main quantitative result of this paper, we first must choose what components  $E_i^2$  and  $B_i^2$  we adopt as probability density  $F^2$ . Note all components have a similar behavior, and thus we can choose their most favorable linear combination. We opt for the Lagrangian density  $\mathcal{L}$  in Eq. (10), which has a better signal-to-noise ratio.

Moreover, we must select the interval  $[0, r_{\max}]$  in the distance  $r$  where we fit the profile of the flux tube. This leads to a systematic error, as in Ref. [81–83]. The profile vanishes at least exponentially with distance, the points

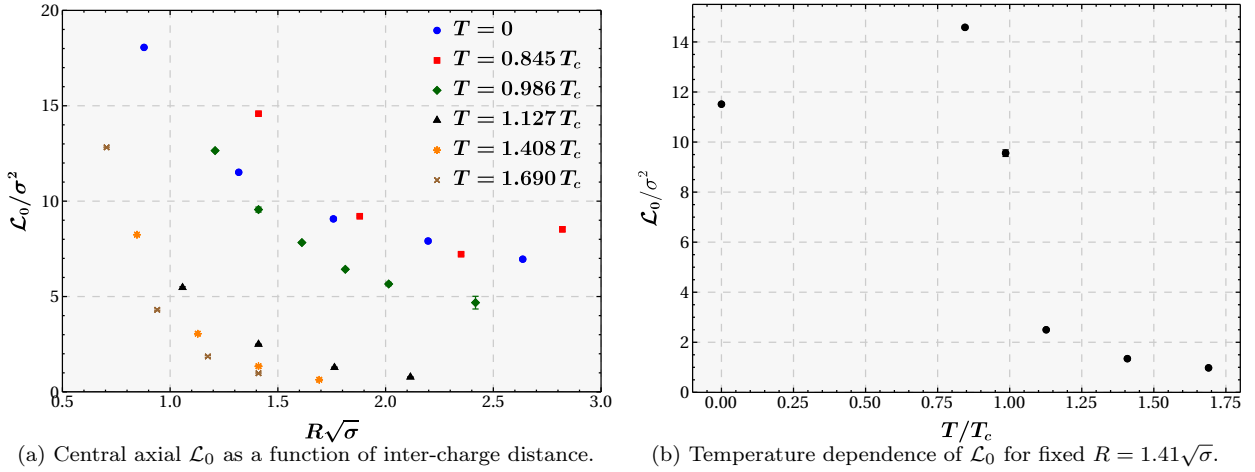


Figure 8: (Colour Online.) Axial value of the Lagrangian  $\mathcal{L}_0$  as a function of the  $Q\bar{Q}$  inter-charge distance  $R$  in string tension units, for the different temperatures. The error bars are total error bars, including both statistical and systematic errors.

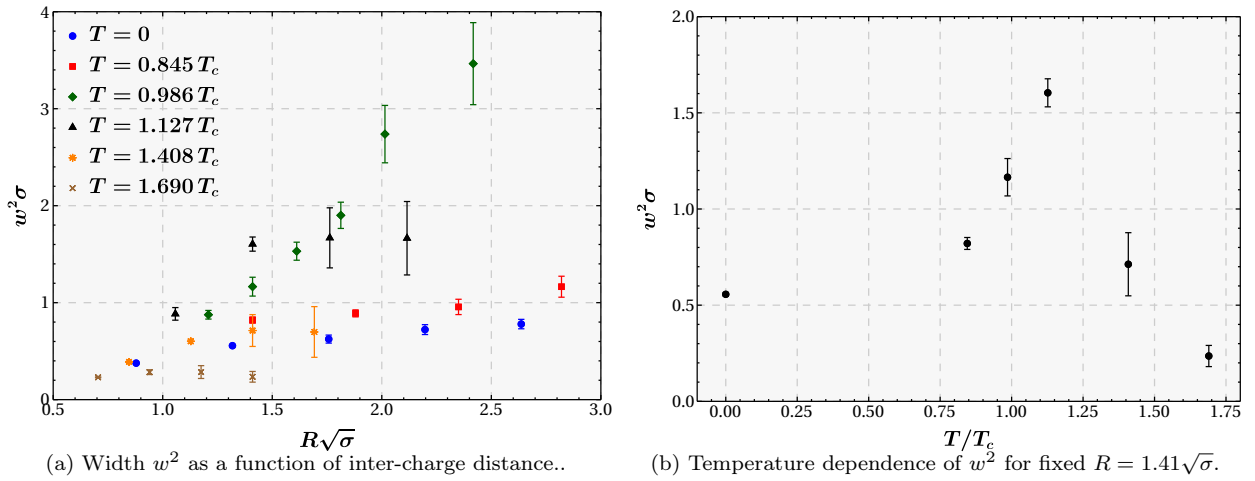


Figure 9: (Colour Online.) Flux tube width  $w^2$  as a function of the  $Q\bar{Q}$  inter-charge distance  $R$  in string tension units, for the different temperatures. The error bars are total error bars, including both statistical and systematic errors.

with larger  $r$  correspond to a vanishing profile, with no relevant physical information. Moreover, the statistical error increases with distance, thus we do not need to include them in the fit. We estimate the best interval is the one where  $r_{\max}$  corresponds to a value for the Lagrangian density between  $\mathcal{L}_0/50$  and  $\mathcal{L}_0/500$ . For instance, in the case of a Gaussian distribution, this would correspond to a confidence level between 99,5 % and 99,96 %.

To extract the width from the Lagrangian density, as illustrated in Fig. 7, we proceed as follows. We crudely estimate  $\mathcal{L}_0$  from the point in the charge axis, at  $r = 0$ . We fit the Lagrangian density with our ansatz in Eq. (12), with  $r_{\max}$  in the interval between  $\mathcal{L}_0/50$  and  $\mathcal{L}_0/500$  crudely estimated. With our fit we then get a correct estimate of  $\mathcal{L}_0$ ,  $\mathcal{L}_0/50$  and  $\mathcal{L}_0/500$ , and redo our fits with the correct  $r_{\max}$ . Then, for all possible different intervals

with  $r_{\max} \in [\mathcal{L}_0/50, \mathcal{L}_0/500]$ , and respective fits of  $\mathcal{L}$ , we determine the parameters  $F_0^2 = \mathcal{L}_0$ ,  $\lambda$ ,  $\nu$  and  $w^2$ .

The parameters come with a statistical error from each fit range  $[0, r_{\max}]$ . Moreover, combining all fit ranges, we obtain a systematic error [81–83]. We obtain a barycenter for the systematic error value, and two different upper and lower error bars considering the maximum differences to the barycenter. Finally, for the total error bars, the systematic upper and lower error are averaged, and combined with the statistical error to provide a total error. In Table II we detail the statistical, systematic and total error bars in the case of  $\beta = 5.96$ .

Unfortunately, our data is not precise enough to determine both the parameters  $\lambda$  and  $\nu$  with small error bars. In some of our cases, these two parameters have large statistical error bars, due to redundancy. To remove the

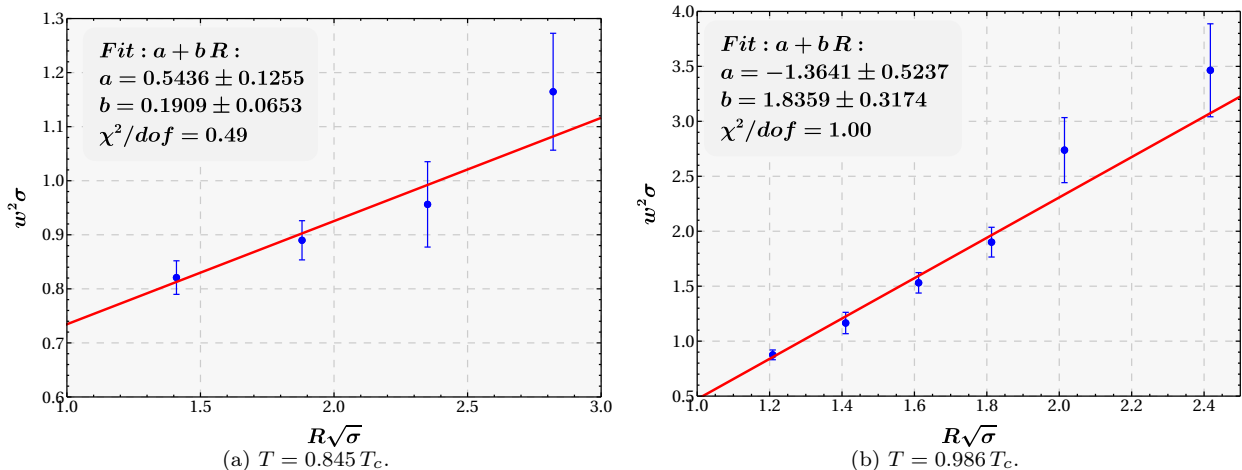


Figure 10: (Colour Online.) Results with combined statistical and systematic errors, at finite temperature below  $T_c$ , for the widening of the flux tube as a function of the intercharge  $Q\bar{Q}$  distance.

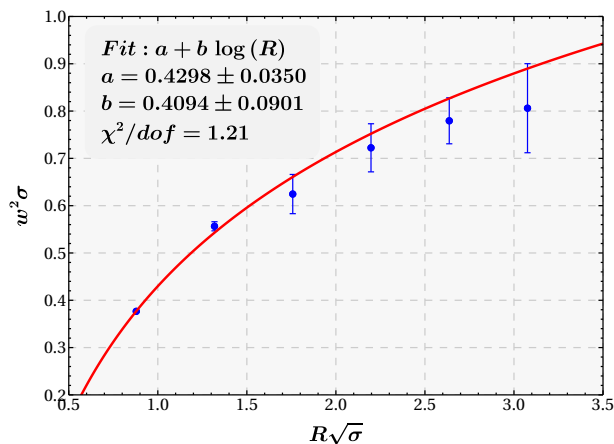


Figure 11: (Colour Online.) Results with combined statistical and systematic errors, at vanishing  $T = 0$ , for the widening of the flux tube as a function of the intercharge  $Q\bar{Q}$  distance.

redundancy, we would need more data, in order to reduce the statistical error bars.

Nevertheless, the central value parameter  $\mathcal{L}_0$  and the width  $w$  have small statistical error bars, and we show them in Figs. 8 and 9. It is clear the central value of the flux tube density  $\mathcal{L}_0$  rapidly decreases with temperatures above  $T_c$ . Moreover there is no evidence for widening at temperatures above  $T_c$  since the width is essentially constant with distance.

Finally, we plot the square widths  $w^2$ , for every temperature below  $T_c$ , as a function of the  $Q\bar{Q}$  intercharge distance  $R$ , in Figs. 10 and 11. For the finite  $0 < T < T_c$  data computed here, we find a new behavior. Indeed the data is consistent with a linear fit, as predicted by Ref. [72]. We also reanalyze the data of Ref. [42] for  $T = 0$  with the present technique to compute the systematic errors, in Fig. 11, and we confirm the logarithmic behavior

of the width.

## V. CONCLUSIONS

Using CUDA codes and computations in NVIDIA GPUs only, we compute the square densities of the chromomagnetic and chromoelectric fields produced by different Polyakov loop sources, above and below the phase transition. We fit the profile of the flux tubes and compute physical parameters, including the flux tube width, with statistical and systematic errors.

As the distance increase between the sources, the fields square densities decrease. Below the deconfinement critical temperature, this decrease is moderate and is consistent with the widening of the flux tube as already seen in studies at zero temperature [42], moreover the field strength clearly decreases as the temperature increases as expected from the critical curve for the string tension [43].

Above the deconfinement critical temperature, at  $T > T_c$ , the fields rapidly decrease to zero as the quarks are pulled apart, qualitatively consistent with screened Coulomb-like fields. While the width of the flux tube below the phase transition temperature increases with the separation between the quark-antiquark, above the phase transition we find no evidence for widening. Moreover, the squared field densities are additive, in the sense the fields produced by a quark  $Q$ , an antiquark  $\bar{Q}$  and a gluon  $G$  approximately add up together when these sources coexist. In the same perspective, the  $QQ$  and the  $Q\bar{Q}$  square fields are essentially similar. This is in contradiction with the squeezing of the fields into a flux tube which should be non-linear. Thus we find evidence for the non-existence of flux tubes at temperature above the deconfinement temperature,  $T > T_c$ .

As an outlook, we plan to complete the present study with further tests of the additive nature of squared field



densities above  $T_c$ . We also would like to produce results with smaller error bars, in order to be able to measure precisely the penetration length parameter  $\lambda$  at finite  $T$ , as we did for vanishing  $T$  in Ref. [42]. We also plan to produce the different Polyakov loop - Polyakov loop potentials, relevant for the modeling of the deconfinement transition [84–86].

## ACKNOWLEDGMENTS

Nuno Cardoso and Marco Cardoso are supported by FCT under the contracts SFRH/BPD/109443/2015

and SFRH/BPD/73140/2010 respectively. We also acknowledge the use of CPU and GPU servers of PtQCD, supported by NVIDIA, CFTP and FCT grant UID/FIS/00777/2013.

- 
- [1] A. Di Giacomo, M. Maggiore, and S. Olejnik, Phys. Lett. **B236**, 199 (1990).
  - [2] A. Di Giacomo, M. Maggiore, and S. Olejnik, Nucl. Phys. **B347**, 441 (1990).
  - [3] V. Singh, D. A. Browne, and R. W. Haymaker, Phys. Lett. **B306**, 115 (1993), arXiv:hep-lat/9301004 [hep-lat].
  - [4] G. S. Bali, K. Schilling, and C. Schlichter, Phys. Rev. **D51**, 5165 (1995), arXiv:hep-lat/9409005.
  - [5] T. Regge, Nuovo Cim. **14**, 951 (1959).
  - [6] T. Regge, Nuovo Cim. **18**, 947 (1960).
  - [7] P. D. B. Collins, *An Introduction to Regge Theory and High-Energy Physics*, Cambridge Monographs on Mathematical Physics (Cambridge Univ. Press, Cambridge, UK, 2009).
  - [8] A. B. Kaidalov, (2001), arXiv:hep-ph/0103011.
  - [9] D. V. Bugg, Phys. Rept. **397**, 257 (2004), arXiv:hep-ex/0412045 [hep-ex].
  - [10] M. Cardoso, N. Cardoso, and P. Bicudo, Phys. Rev. **D81**, 034504 (2010), arXiv:0912.3181 [hep-lat].
  - [11] N. Cardoso, M. Cardoso, and P. Bicudo, Phys. Rev. **D84**, 054508 (2011), arXiv:1107.1355 [hep-lat].
  - [12] N. Cardoso, M. Cardoso, and P. Bicudo, Phys. Lett. **B710**, 343 (2012), arXiv:1108.1542 [hep-lat].
  - [13] N. Cardoso and P. Bicudo, Phys. Rev. **D87**, 034504 (2013), arXiv:1209.1532 [hep-lat].
  - [14] A. M. Polyakov, Phys. Lett. **B59**, 82 (1975).
  - [15] T. Banks, R. Myerson, and J. B. Kogut, Nucl. Phys. **B129**, 493 (1977).
  - [16] J. Smit and A. van der Sijs, Nucl. Phys. **B355**, 603 (1991).
  - [17] G. S. Bali, V. Bornyakov, M. Muller-Preussker, and K. Schilling, Phys. Rev. **D54**, 2863 (1996), arXiv:hep-lat/9603012.
  - [18] F. Gubarev, E.-M. Ilgenfritz, M. Polikarpov, and T. Suzuki, Phys. Lett. **B468**, 134 (1999), arXiv:hep-lat/9909099 [hep-lat].
  - [19] Y. Koma, M. Koma, E.-M. Ilgenfritz, T. Suzuki, and M. Polikarpov, Phys. Rev. **D68**, 094018 (2003), arXiv:hep-lat/0302006 [hep-lat].
  - [20] M. Chernodub, K. Ishiguro, Y. Mori, Y. Nakamura, M. Polikarpov, *et al.*, Phys. Rev. **D72**, 074505 (2005), arXiv:hep-lat/0508004 [hep-lat].
  - [21] Y. Nambu, Phys. Rev. **D10**, 4262 (1974).
  - [22] G. 't Hooft, Nucl. Phys. **B153**, 141 (1979).
  - [23] S. Mandelstam, Phys. Rept. **23**, 245 (1976).
  - [24] M. Baker, J. S. Ball, and F. Zachariasen, Phys. Rev. **D41**, 2612 (1990).
  - [25] M. Baker, J. S. Ball, and F. Zachariasen, Phys. Rept. **209**, 73 (1991).
  - [26] A. A. Abrikosov, Sov. Phys. JETP **5**, 1174 (1957).
  - [27] H. B. Nielsen and P. Olesen, Nucl. Phys. **B61**, 45 (1973).
  - [28] M. Cardoso, P. Bicudo, and P. D. Sacramento, arXiv:hep-ph/0607218v1 (2006).
  - [29] Y. V. Burdanov, G. V. Efimov, and S. N. Nedelko, (1998), arXiv:hep-ph/9806478.
  - [30] D. Jia, (2005), arXiv:hep-th/0509030.
  - [31] T. Suzuki, K. Ishiguro, Y. Mori, and T. Sekido, AIP Conf. Proc. **756**, 172 (2005), arXiv:hep-lat/0410039.
  - [32] H. Suganuma, K. Amemiya, H. Ichie, and Y. Koma, (2004), arXiv:hep-ph/0407121.
  - [33] H. Suganuma *et al.*, (2004), arXiv:hep-lat/0407020.
  - [34] H. Suganuma and H. Ichie, Nucl. Phys. Proc. Suppl. **121**, 316 (2003), arXiv:hep-lat/0407012.
  - [35] A. Kumar and R. Parthasarathy, Phys. Lett. **B595**, 373 (2004), arXiv:hep-th/0406033.
  - [36] J. V. Burdanov and G. V. Efimov, (2002), arXiv:hep-ph/0209285.
  - [37] N. Cardoso, M. Cardoso, and P. Bicudo, (2010), arXiv:1004.0166 [hep-lat].
  - [38] O. Oliveira and P. Bicudo, (2010), arXiv:1002.4151 [hep-lat].
  - [39] P. Bicudo, F. Giacosa, and E. Seel, Phys. Rev. **C86**, 034907 (2012), arXiv:1202.1640 [hep-ph].
  - [40] M. S. Cardaci, P. Cea, L. Cosmai, R. Falcone, and A. Papa, Phys. Rev. **D83**, 014502 (2011), arXiv:1011.5803 [hep-lat].
  - [41] P. Cea, L. Cosmai, and A. Papa, Phys. Rev. **D86**, 054501 (2012), arXiv:1208.1362 [hep-lat].
  - [42] N. Cardoso, M. Cardoso, and P. Bicudo, Phys. Rev. **D88**, 054504 (2013), arXiv:1302.3633 [hep-lat].
  - [43] N. Cardoso and P. Bicudo, Phys. Rev. **D85**, 077501 (2012), arXiv:1111.1317 [hep-lat].
  - [44] R. G. Edwards, U. M. Heller, and T. R. Klassen, Nucl. Phys. **B517**, 377 (1998), arXiv:hep-lat/9711003.
  - [45] M. Luscher, G. Munster, and P. Weisz, Nucl. Phys. **B180**, 1 (1981).
  - [46] G. Munster and P. Weisz, Nucl. Phys. **B180**, 13 (1981).
  - [47] Y. Nambu, Phys. Lett. **B80**, 372 (1979).
  - [48] T. Goto, Prog. Theor. Phys. **46**, 1560 (1971).
  - [49] M. Luscher, Nucl. Phys. **B180**, 317 (1981).

- [50] J. F. Arvis, Phys. Lett. **B127**, 106 (1983).
- [51] F. Gliozzi, M. Pepe, and U.-J. Wiese, JHEP **1011**, 053 (2010), arXiv:1006.2252 [hep-lat].
- [52] A. Amado, N. Cardoso, M. Cardoso, and P. Bicudo, (2012), arXiv:1208.0166 [hep-lat].
- [53] A. Armoni and J. M. Ridgway, Nucl.Phys. **B801**, 118 (2008), arXiv:0803.2409 [hep-th].
- [54] V. Bornyakov, A. Kovalenko, M. Polikarpov, and D. Sigaev, Nucl.Phys.Proc.Suppl. **119**, 739 (2003), arXiv:hep-lat/0209029 [hep-lat].
- [55] V. Bornyakov, A. Kovalenko, M. Polikarpov, and D. Sigaev, Nucl.Phys.Proc.Suppl. **129**, 757 (2004), arXiv:hep-lat/0309049 [hep-lat].
- [56] M. Cardoso, P. Bicudo, and N. Cardoso, (2012), arXiv:1208.2552 [hep-lat].
- [57] M. Caselle, F. Gliozzi, U. Magnea, and S. Vinti, Nucl.Phys. **B460**, 397 (1996), arXiv:hep-lat/9510019 [hep-lat].
- [58] M. Caselle, JHEP **1008**, 063 (2010), arXiv:1004.3875 [hep-lat].
- [59] M. Caselle and P. Grinza, (2012), arXiv:1207.6523 [hep-th].
- [60] M. Chernodub and F. Gubarev, Phys.Rev. **D76**, 016003 (2007), arXiv:hep-lat/0703007 [HEP-LAT].
- [61] P. Giudice, F. Gliozzi, and S. Lottini, PoS **LAT2006**, 070 (2006), arXiv:hep-lat/0609060 [hep-lat].
- [62] P. Giudice, F. Gliozzi, and S. Lottini, JHEP **0701**, 084 (2007), arXiv:hep-th/0612131 [hep-th].
- [63] F. Gliozzi, (2006), arXiv:hep-lat/0601011 [hep-lat].
- [64] F. Gliozzi, (1994), arXiv:hep-lat/9410022 [hep-lat].
- [65] F. Gliozzi, M. Pepe, and U.-J. Wiese, JHEP **1101**, 057 (2011), arXiv:1010.1373 [hep-lat].
- [66] F. Gliozzi, M. Pepe, and U.-J. Wiese, Phys.Rev.Lett. **104**, 232001 (2010), arXiv:1002.4888 [hep-lat].
- [67] J. Greensite and P. Olesen, JHEP **0011**, 030 (2000), arXiv:hep-th/0008080 [hep-th].
- [68] B. Lucini and M. Teper, Phys.Rev. **D64**, 105019 (2001), arXiv:hep-lat/0107007 [hep-lat].
- [69] H. B. Meyer, Phys.Rev. **D82**, 106001 (2010), arXiv:1008.1178 [hep-lat].
- [70] A. Bakry, D. Leinweber, P. Moran, A. Sternbeck, and A. Williams, Phys.Rev. **D82**, 094503 (2010), arXiv:1004.0782 [hep-lat].
- [71] A. S. Bakry, D. B. Leinweber, and A. G. Williams, Phys.Rev. **D85**, 034504 (2012), arXiv:1011.1380 [hep-lat].
- [72] A. Allais and M. Caselle, JHEP **01**, 073 (2009), arXiv:0812.0284 [hep-lat].
- [73] A. S. Bakry, X. Chen, and P.-M. Zhang, Phys. Rev. **D91**, 114506 (2015), arXiv:1412.3568 [hep-lat].
- [74] A. S. Bakry, D. B. Leinweber, and A. G. Williams, Phys. Rev. **D91**, 094512 (2015), arXiv:1107.0150 [hep-lat].
- [75] A. Shibata, K.-I. Kondo, S. Kato, and T. Shinohara, in *Sakata Memorial KMI Workshop on Origin of Mass and Strong Coupling Gauge Theories (SCGT15) Nagoya, Japan, March 3-6, 2015* (2015) arXiv:1511.04155 [hep-lat].
- [76] P. Cea, L. Cosmai, F. Cuteri, and A. Papa, JHEP **06**, 033 (2016), arXiv:1511.01783 [hep-lat].
- [77] O. Kaczmarek, F. Karsch, E. Laermann, and M. Lutgemeier, Phys. Rev. **D62**, 034021 (2000), arXiv:hep-lat/9908010.
- [78] Y.-c. Peng and R. W. Haymaker, Phys. Rev. **D47**, 5104 (1993), arXiv:hep-lat/9302009 [hep-lat].
- [79] R. Brower, P. Rossi, and C.-I. Tan, Nucl. Phys. **B190**, 699 (1981).
- [80] G. Parisi, R. Petronzio, and F. Rapuano, Phys.Lett. **B128**, 418 (1983).
- [81] K. Cichy, V. Drach, E. Garcia-Ramos, G. Herdoiza, and K. Jansen, Nucl. Phys. **B869**, 131 (2013), arXiv:1211.1605 [hep-lat].
- [82] P. Bicudo, K. Cichy, A. Peters, B. Wagenbach, and M. Wagner, Phys. Rev. **D92**, 014507 (2015), arXiv:1505.00613 [hep-lat].
- [83] P. Bicudo, K. Cichy, A. Peters, and M. Wagner, Phys. Rev. **D93**, 034501 (2016), arXiv:1510.03441 [hep-lat].
- [84] D. Smith, A. Dumitru, R. Pisarski, and L. von Smekal, Phys. Rev. **D88**, 054020 (2013), arXiv:1307.6339 [hep-lat].
- [85] P. Bicudo, R. D. Pisarski, and E. Seel, Phys. Rev. **D89**, 085020 (2014), arXiv:1402.5137 [hep-ph].
- [86] J. Greensite and K. Langfeld, Phys. Rev. **D90**, 014507 (2014), arXiv:1403.5844 [hep-lat].